Available online at www.sciencedirect.com
ScienceDirect
Trans. Nonferrous Met. Soc. China 30(2020) 2035−2044
Transactions of Nonferrous Metals Society of China
www.tnmsc.cn

Kinetic behaviour of TiB_2 particles in Al melt and their effect on grain refinement of aluminium alloys

Li-li ZHANG[1], Hong-xiang JIANG[1], Jie HE[1,2], Jiu-zhou ZHAO[1,2]

1. Shi-changxu Innovation Center for Advanced Materials, Institute of Metal Research, Chinese Academy of Sciences, Shenyang 110016, China;
2. School of Materials Science and Engineering, University of Science and Technology of China, Shenyang 110016, China

Received 29 November 2019; accepted 28 June 2020

Abstract: Solidification experiments were carried out to investigate the kinetic behaviour of TiB_2 particles in Al melt and their effect on the grain refinement of commercially-pure Al. A model was proposed to describe the kinetic behaviour of TiB_2 particles during the whole process from the addition of TiB_2 to the melt to the freezing of the melt. The results indicate that TiB_2 particles are not stable in Al melt. They may dissolve and coarsen during the holding period and grow during the cooling period of the melt. The kinetic behaviour of TiB_2 particles in the melt has a great influence on their number density and the grain refinement. Solute Ti addition can suppress the dissolution, Ostwald ripening and growth behaviours of TiB_2 particles.
Key words: TiB_2 particles; kinetic behaviour; grain refinement; aluminium alloy

1 Introduction

To achieve a fine equiaxed grain structure has attracted much attention in the industrial production [1−5]. Many techniques have been developed to refine the microstructures nowadays, among which inoculation is the most popular one. Al−Ti−B master alloys are widely used as the grain refiners for aluminium alloys [6−9].

Models have been built to describe the microstructure formation of aluminium alloys under the effect of Al−Ti−B master alloys since the 1970s. MAXWELL and HELLAWELL [10] developed a numerical approach to predict the grain size assuming that the nucleation of α(Al) occurred in an isothermal melt and concluded that the recalescence was the key factor to stifle the nucleation process. GREER et al [11] proposed a free-growth model suggesting that α(Al) could freely grow and form a grain only on the TiB_2 particle of the size larger than the critical nucleus of α(Al). Based on this model, QUESTED and GREER [12,13] quantitatively predicted the grain size of aluminium alloys inoculated with Al−5Ti−1B (wt.%, the same as below unless otherwise specified) master alloy. During the year of 2005−2008, EASTON and STJOHN [14−16] proposed a semi-empirical equation to predict the grain size of aluminium alloys. In 2010, an analytical model was presented for the constitutional supercooling-driven grain formation. It linked the nucleation of a grain to the growth of a larger neighbouring grain [17]. These researches clearly demonstrate that the grain refinement is closely related to the number density and size distribution of the TiB_2 particles as well as

Foundation item: Projects (51901231, 51971227, 51771210, 51774264) supported by the National Natural Science Foundation of China; Project (2019-BS-253) supported by the Natural Science Foundation of Liaoning Province, China
Corresponding author: Li-li ZHANG, Tel: +86-24-23971905, E-mail: llzhang@imr.ac.cn;
Jiu-zhou ZHAO, Tel: +86-24-23971918, E-mail: jzzhao@imr.ac.cn
DOI: 10.1016/S1003-6326(20)65358-4

the solute Ti concentration in the melt. It is believed that TiB_2 particles act as the substrates for heterogeneous nucleation of α(Al) grains, while the solute Ti affects the microstructure formation through restricting the growth of α(Al) grains. The growth rate of α(Al) grains is inversely proportional to the growth restriction factor Q_{Ti}, which is related to the solute Ti concentration in the Al melt (c_{Ti0}) by [18,19]

$$Q_{Ti}=c_{Ti0}m_{Ti}(k_{Ti}-1) \quad (1)$$

where m_{Ti} (=33.3 K/wt.%) and k_{Ti} (=7.80) are the liquidus slope and equilibrium partition coefficient in the Al−Ti phase diagram, respectively [14].

Although considerable progress has been made in the research on the microstructure formation of the aluminium alloys under the effect of Al−Ti−B master alloys, there still exist scientific problems to be resolved, such as the kinetic behaviour of TiB_2 particles in the Al melt and its effect on the grain refinement of aluminium alloys. In the previous modelling and simulation of the solidification of aluminium alloys, it was generally assumed that TiB_2 particles were stable in Al melt and their sizes did not change. In fact, although the solubility product $K^{\theta}_{TiB_2}$ is quite small [20], TiB_2 particles may dissolve and coarsen during the holding period and even precipitate during the cooling period of the melt, which leads to a change in the size distribution of TiB_2 particles and the grain refinement. This work will investigate the kinetic behaviour of TiB_2 particles in Al melt and its effect on the grain refinement of aluminium alloys. This may contribute to the exploration of the real microstructure evolution of aluminium alloys with the addition of Al−Ti−B master alloys and to the development of the high-quality grain refiners.

2 Experimental

2.1 Materials

Commercially-pure Al (CP-Al, 99.7%), Al−3.6Ti−1.2B and Al−3Ti master alloys were used as the raw materials. The chemical composition of the CP-Al is given in Table 1. Al−3.6Ti−1.2B master alloy was used to provide TiB_2 particles and Al−3Ti master alloy was used to vary the solute Ti concentration.

Table 1 Values of concentration c_0, equilibrium partition coefficient k and liquidus slope m [14] for impurity elements in CP-Al used in present work

Element	c_0/wt%	k	m/(K·wt.%$^{-1}$)
Fe	0.14	0.03	−2.925
Si	0.08	0.12	−6.62
Ga	0.014	0.14	−2.52
Mg	0.003	0.51	−6.2
Cu	0.001	0.17	−3.4
Mn	0.001	0.94	−1.6

2.2 Experiments for examining kinetic behaviour of TiB_2 particles

CP-Al was first melted and heated to 1123 K in a corundum crucible using an electric resistance furnace. Then, 10% Al−3.6Ti−1.2B master alloy was added to the melt. After that, the melt was stirred and held at 1123 K for 30, 60, 90 and 120 min, respectively. Finally, the melt was solidified at a cooling rate of about 50 K/s.

2.3 Grain refinement experiments

CP-Al was first melted and heated to 983 K in a corundum crucible using an electric resistance furnace. Then, 0.0154% TiB_2 particles and different amounts of solute Ti were added to the melt by using the master alloys. After that, the melt was stirred and held at 983 K for different time. Finally, the melt was poured into a cast-iron mould pre-heated to 423 K to form a frustum ingot with a height of 120 mm and the top and bottom diameters of 50 and 10 mm, respectively. A tungsten−rhenium thermocouple was situated at the centre of the section approximately 20 mm from the base of the mould to monitor the melt temperature. The cooling rate of the melt in the temperature range from 983 K to the freezing point of α(Al) (T_m) was about 15 K/s.

Two groups of experiments were respectively carried out to investigate the effect of solute Ti content on the grain refinement (Group 1 in Table 2) and the fading phenomenon of grain refinement (Group 2 in Table 2).

2.4 Sample characterization

The microstructures of Al−Ti−B and Al−3Ti master alloys were characterised by using the field-emission scanning electron microscopy (FESEM).

Table 2 Experimental parameters and average size of α(Al) grains

Group No.	Addition level/%		Holding time of melt/min	Average size of α(Al) grains/μm
	Al−3.6Ti−1.2B (TiB_2+Ti)	Al−3Ti (Ti)		
1	0.4 (0.0154TiB_2+0.0038Ti)	0	15	114.7
		0.11 (0.0033)		107.8
		0.33 (0.0099)		91.3
		0.43 (0.0129)		90.5
		0.54 (0.0162)		88.4
2	0.4 (0.0154TiB_2+0.0038Ti)	0	15	114.7
			30	117.8
			60	127.4
			90	131.2

The average grain size of commercially-pure Al is 753.0 μm

The TiB_2 particle in the master alloys, which is in fact hexagonal with the height/diameter ratio of about 0.35 [13], is treated as a sphere in this work. The size distribution of the TiB_2 particles was analyzed by using the following procedure: First, randomly select about 500 particles for each sample and measure the longest dimension d of (0001) face for each particle by using the SISC IAS V8.0 software; Then, determine the radius R of the equivalent sphere by using volume equivalent principle (Eq. (2)); Finally, calculate the number density of TiB_2 particles in the alloy based on their volume fraction, which is the sum of each particle volume over the radius range:

$$\frac{4}{3}\pi R^3 = \left(d+\frac{d}{2}\right)\frac{\sqrt{3}}{2}\frac{d}{2}\frac{35d}{100} \quad (2)$$

The frustum ingots were sectioned approximately 20 mm from the bottom. The sections were ground, polished electrolytically for about 50 s at 30 V in a reagent of 90 mL CH_3CH_2OH + 10 mL $HClO_4$ and anodized for about 120 s at 20 V in Barker's reagent (2.5 mL HBF_4 + 97.5 mL distilled water) to prepare the metallographic specimens. The microstructures were examined using a Zeiss optical microscope with polarized light. The average size (two-dimensional, the same as below) of α(Al) grains which were taken from the central region of the cross-section was determined by using the SISC IAS V8.0 software.

3 Results

3.1 Microstructures of master alloys

The microstructures of the master alloys used in the present work are shown in Fig. 1. The results indicate that Al−3.6Ti−1.2B master alloy consists of Al matrix, TiB_2 and a few of $TiAl_3$ phases. The radius of TiB_2 particles is in a range 0.15−0.55 μm. The average radius and number density of the TiB_2 particles are about 0.33 μm and 1.15×10^{17} m^{-3}, respectively.

3.2 Change of TiB_2 particle size in Al melt

Figure 2 shows the average radius of the TiB_2 particles in the CP-Al with 10% addition of Al−3.6Ti−1.2B master alloy and solidified at a cooling rate of 50 K/s after holding at 1123 K for different time. It is demonstrated that TiB_2 particles are unstable in Al melt. The average radius of the TiB_2 particles increases with prolonging the holding time of the melt.

3.3 Grain refinement of CP-Al

Figure 3 shows the optical micrographs of the CP-Al without inoculation and inoculated with 0.4% Al−3.6Ti−1.2B and different additions of Al−3Ti master alloys (Group 1 in Table 2). The average sizes of α(Al) grains in these CP-Al samples are given in Table 2. It is indicated that the α(Al) grains are significantly refined by the addition of 0.0154% TiB_2 particles. The grain size decreases further with the solute Ti content up to 0.0137%. After that, the grain size almost no longer decreases with ulteriorly increasing the solute Ti content.

The dependence of the average size of α(Al) grains on the holding time of the melt is shown in Table 2. It is demonstrated that the fading of grain refinement increases with prolonging the holding time of the melt.

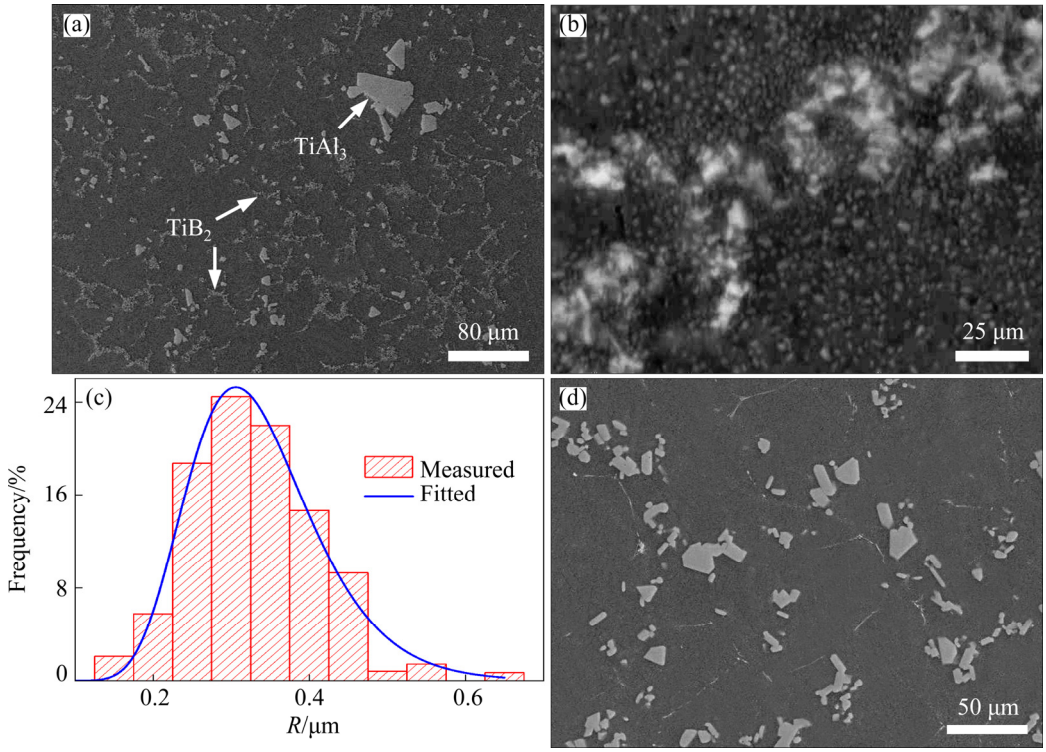

Fig. 1 FESEM images of Al−3.6Ti−1.2B alloy at low (a) and high (b) magnifications, size distribution of TiB_2 particles in Al−3.6Ti−1.2B alloy (c) and FESEM image of Al−3Ti alloy (d)

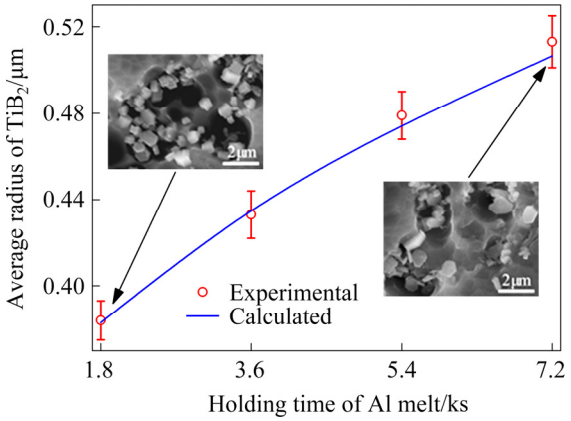

Fig. 2 Experimental and calculated average radius of TiB_2 particles vs holding time of melt at 1123 K (Insets show FESEM images of TiB_2 particles)

4 Discussion

4.1 Kinetic behaviour of TiB_2 particles in Al melt

4.1.1 Theoretical model for kinetic behaviour of TiB_2 particles in Al melt

A model, based on the population dynamic approach [21], is proposed to investigate the kinetic behaviour of TiB_2 particles in Al melt during the whole process from the addition of TiB_2 to the freezing of the melt. A function $f(R,t)$ is defined to describe the size distribution of TiB_2 particles with t being the time. $f(R,t)\mathrm{d}R$ gives the number density of TiB_2 particles in a radius range R−(R+dR) at time t. According to the definition of $f(R,t)$, the number density N, average radius $\bar{R}$ and volume fraction φ of TiB_2 particles in the melt can be respectively calculated by the following equations:

$$N=\int_0^{\infty} f(R,t)\,\mathrm{d}R \tag{3}$$

$$\bar{R}=\frac{1}{N}\int_0^{\infty} Rf(R,t)\,\mathrm{d}R \tag{4}$$

$$\varphi=\frac{4\pi}{3}\int_0^{\infty} R^3 f(R,t)\,\mathrm{d}R \tag{5}$$

Taking into consideration the common actions of the nucleation and growth/dissolution of the TiB_2 particles, $f(R,t)$ obeys the following continuity equation [22,23]:

$$\frac{\partial f(R,t)}{\partial t}+\frac{\partial\left[vf(R,t)\right]}{\partial R}=\left.\frac{\partial I}{\partial R}\right|_{R=R^*} \tag{6}$$

where $\partial f(R,t)/\partial t$ describes the time dependence of $f(R,t)$, $\partial[vf(R,t)]/\partial R$ reflects the contribution of the growth/dissolution of TiB_2 particles with v being the growth/dissolution rate of TiB_2 particles, and $\partial I/\partial R|_{R=R^*}$ is the source term due to the nucleation of TiB_2 particles with I and R^* being the nucleation

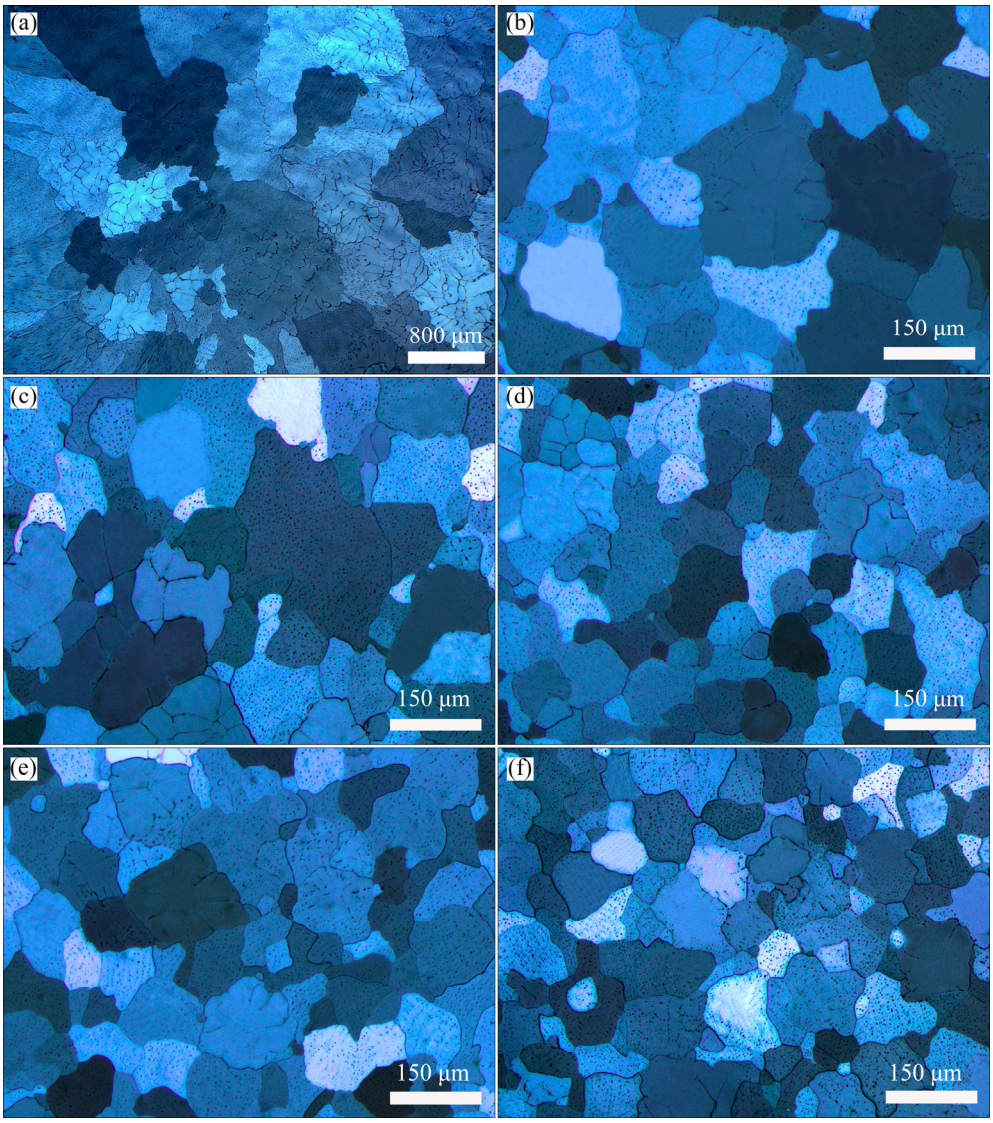

Fig. 3 Optical micrographs of CP-Al without inoculation (a) and inoculated with 0.0154% TiB_2 particles and 0.0038% (b), 0.0071% (c), 0.0137% (d), 0.0167% (e) and 0.0200% (f) solute Ti

rate and the critical nucleation radius of TiB_2 particles, respectively.

TiB_2 particles embedded in supersaturated/unsaturated Al melt will grow/dissolve by the diffusional transport of solutes Ti and B. Under the present experimental conditions, the growth/dissolution process of TiB_2 particles is controlled by the diffusion of solute B because, on one hand, the mole fraction of solute B is much lower than that of solute Ti and, on the other hand, the growth/dissolution of a TiB_2 particle costs more B atoms. The growth/dissolution rate of TiB_2 particles can be calculated by [24]

$$v = -D_B \frac{K_B}{R} \tag{7}$$

where D_B is the diffusion coefficient of solute B in the Al melt, $K_B(=(x_B^i - x_B^m)/[(V_{Al}/V_{TiB_2})x_B^s - x_B^i])$ is dimensionless concentration, $x_B^i(\approx\sqrt{K_{TiB_2}^{\theta}/x_{Ti}^m}\cdot\exp(\alpha/R))$ is the mole fraction of solute B in the Al melt at the Al(l)/TiB_2(s) interface, x_{Ti}^m and x_B^m are respectively the mole fractions of solutes Ti and B in the Al melt, $\alpha(=(2\gamma_{Al(l)/TiB_2(s)}V_{TiB_2})/(R_gT))$ is the capillary length, $\gamma_{Al(l)/TiB_2(s)}$ (≈0.853 J/m^2 [25]) is the Al(l)/TiB_2(s) interfacial energy, V_{Al}(=1.13×10^{-5} m^3/mol [26]) and V_{TiB_2} (=1.55×10^{-5} m^3/mol [27]) are respectively the molar volumes of the Al melt and TiB_2 particles, R_g(=8.314 J/(mol·K)) is the gas constant, T is the thermodynamic temperature, and x_B^s is the mole fraction of solute B in TiB_2 particles.

When the supersaturation of solutes Ti and B in the Al melt is high enough, TiB_2 particles may precipitate out through the following reaction:

$$[Ti]+2[B]\longrightarrow TiB_2(s) \quad (8)$$

where [Ti] and [B] are the solutes Ti and B in the Al melt, respectively.

The nucleation of TiB_2 particles from Al melt can be described by using the classical homogeneous nucleation theory. The nucleation rate I can be calculated by [23]

$$I = N_0' O \Gamma Z \exp\left(-\frac{16\pi\gamma^3_{Al(l)/TiB_2(s)}}{3k_bT\Delta G_v^2}\right) \quad (9)$$

where N_0' is the number density of atoms in the Al melt, $O(=4n_c^{-2/3})$ represents the surface of the nuclei with n_c being the number density of atoms in a TiB_2 particle of the critical radius, $\Gamma(=6D_B/\lambda^2)$ is the transition rate with λ(=2.87 Å [28]) being the average jump distance of a solute atom due to the diffusion, $Z(=(4/3n_c)\cdot\sqrt{\gamma^3_{Al(l)/TiB_2(s)}/(k_bT\Delta G_V^2)})$ is the Zeldovich factor, k_b(=1.38×10^{-23} J/K) is the Boltzmann's constant and $\Delta G_V(=(R_gT/V_{Al})\cdot \ln\{K^{\theta}_{TiB_2}/[(x^m_B)^2x^m_{Ti}]\})$ is the gain in the volume free energy on the nucleation of TiB_2 particles.

The numerical solution method is as follows. The TiB_2 radial axis is divided into a number of intervals (finite volume) with the mesh points located at the centre of each finite volume. The continuity equation is discretized into a set of implicit difference equations with the assumption that the size distribution function of TiB_2 particles varies in a stepwise manner along the direction of the radius axis and also along the time axis. These equations are solved by using the tridiagonal matrix algorithm.

The solubility product of TiB_2 in the Al melt can be calculated by [20]

$$K^{\theta}_{TiB_2} = 10^{3.056-16043/T} \quad (10)$$

The temperature dependence of the diffusion coefficient of solute B in the Al melt is calculated by [29]

$$D_B=D_0T^2 \quad (11)$$

where D_0 is a constant and can be determined by fitting the numerical result with the experimental one.

4.1.2 Numerical results and discussion

The constant D_0 was determined by fitting the numerical result of the average radius of TiB_2 particles in the CP-Al with 10% addition of the Al−3.6Ti−1.2B master alloy and solidified at a cooling rate of 50 K/s after holding for 30 min at 1123 K with the experimental one. That is to say, the kinetic behaviour of the TiB_2 particles in the Al melt is calculated by using different values of D_0 and the one is found out with which the calculated average radius of the TiB_2 particles agrees with the experimental one. The fitting result indicates that D_0 equals 9.0×10^{-17} m^2/(s·K^2). This D_0 is then applied to calculating the kinetic behaviour of TiB_2 particles in the CP-Al with 10% addition of the Al−3.6Ti−1.2B master alloy and solidified at a cooling rate of 50 K/s after holding at 1123 K for other time. The results demonstrate that the numerical results of the average radius of TiB_2 particles agree well with the experimental ones, as shown in Fig. 2.

Figure 4(a) shows the size distributions of the TiB_2 particles in the Al melt with the addition of 0.0154% TiB_2 at different holding time as well as the moment when the melt is cooled to T_m (melting point). Figures 4(b) and (c) show the time dependences of the mole fractions of solutes Ti and B, the supersaturation $\Delta K(=(x^m_B)^2x^m_{Ti}-K^{\theta}_{TiB_2})$ of the melt and the average radius and number density of the TiB_2 particles in the Al melt from the moment when the TiB_2 particles and solute Ti are added to the Al melt at 983 K till the melt is poured into the mould and cooled to T_m. It is demonstrated that the TiB_2 particles, on the addition to the Al melt, are embedded in an unsaturated matrix (ΔK<0) and dissolve in accordance with Eq. (7), resulting in a shift of the peak position of the size distribution to a small size and a decrease in the average radius and the number density of the TiB_2 particles. The dissolution process lasts till $\Delta K\approx0$. Since then, the peak position of the size distribution shifts to a large size and the average radius of the TiB_2 particles increases while the number density decreases with time. Especially in the late stage of the holding period, the average radius and number density of the TiB_2 particles respectively vary with time according to $\bar{R}^3\propto t$ and $N^{-1}\propto t$ (see the inset in Fig. 4(c)), indicating that the TiB_2 particles coarsen through Ostwald ripening [30]. During the

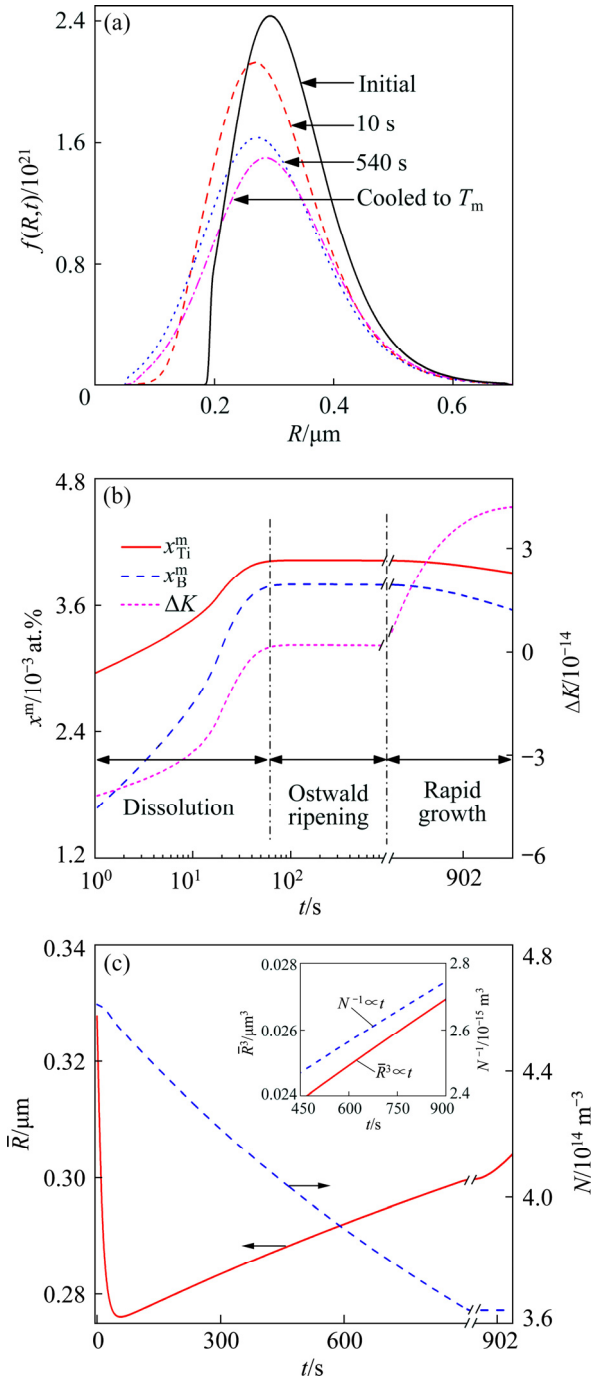

Fig. 4 Size distributions of TiB_2 particles (a), time dependences of solute mole fractions and supersaturation $\Delta K = (x^m_B)^2 x^m_{Ti} - K^\theta_{TiB_2}$ (b), and average radius and number density of TiB_2 particles (c)

cooling of melt, the Ti and B solutes become supersaturated (ΔK>0). The supersaturation is not high enough to cause the nucleation of the TiB_2 particles, but it leads to a rapid growth of the TiB_2 particles in the Al melt. The peak position of the size distribution moves to a larger size and the average radius increases steeply.

Figures 5(a) and (b) show the time dependences of the number density and average radius of the TiB_2 particles in the Al melt inoculated with 0.0154% TiB_2 and different additions of solute Ti. Figure 5(c) shows the size distribution of the TiB_2 particles and Table 3 shows the number density of the TiB_2 particles (N') and the concentration of the solute Ti (c'_{Ti}) in the melt cooled to T_m. It is demonstrated that, on one hand, the N' is quite

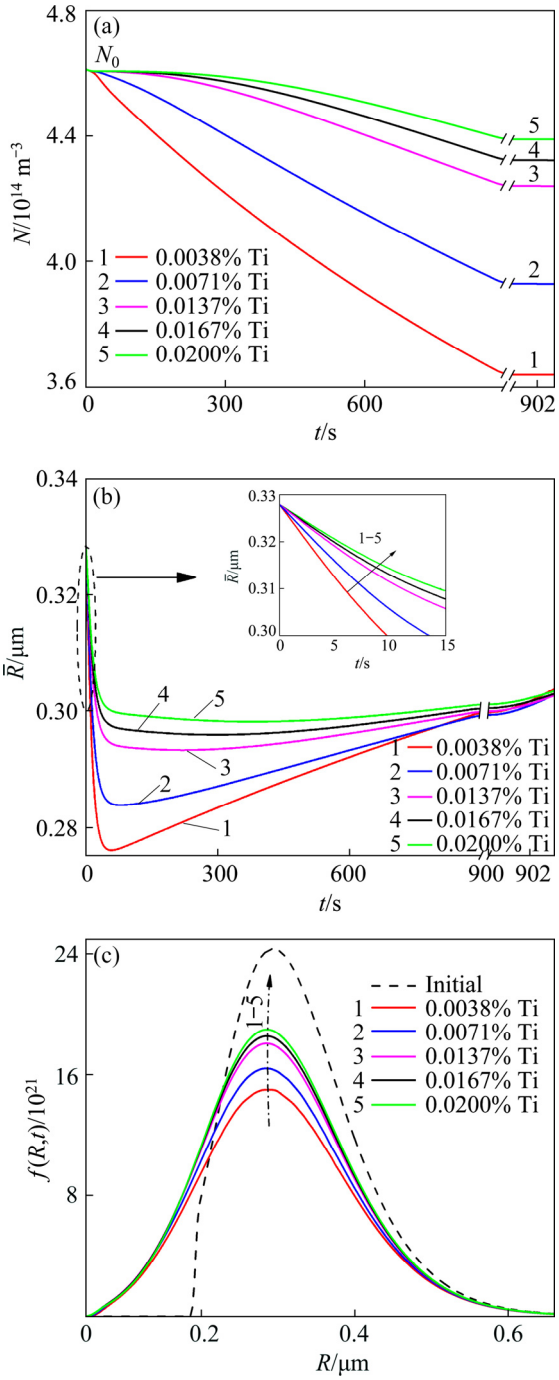

Fig. 5 Time dependences of number density (a) and average radius of TiB_2 particles (b) and size distributions of TiB_2 particles in melt cooled to T_m (c)

Table 3 Calculated results for number density of TiB_2 particles (N'), concentration of solute Ti (c'_{Ti}), growth restriction factor for solute Ti (Q'_{Ti}) and sum of Q values for impurities in CP-Al and solute Ti (Q'_{Total}) in melt cooled to T_m

Group No.	c_{Ti0}/ wt.%	t/ min	N'/ 10^{14} m^{-3}	c'_{Ti}/ wt.%	Q'_{Ti}/ K	Q'_{Total}/ K
1	0.0038	15	3.64	0.0069	1.56	2.47
	0.0071		3.93	0.0098	2.21	3.12
	0.0137		4.24	0.0158	3.57	4.48
	0.0167		4.32	0.0186	4.20	5.11
	0.0200		4.39	0.0218	4.93	5.83
2	0.0038	15	3.64	0.0069	1.56	2.47
		30	3.07	0.0070	1.58	2.49
		60	2.40	0.0070	1.58	2.49
		90	2.00	0.0070	1.58	2.49

different from the N_0 (4.61×10^{14} m^{-3}), which is the initial number density of the TiB_2 added to the melt, indicating that the kinetic behaviour of the TiB_2 particles in the Al melt cannot be negligible. On the other hand, the difference between the N' and N_0 diminishes with the solute Ti content increasing, indicating that the solute Ti can inhibit the dissolution/growth/coarsening behaviours of the TiB_2 particles and the inhibitory effect increases with the solute Ti content increasing.

4.2 Grain refining effect

The average size $\bar{D}$ of α(Al) grains in the aluminium alloys inoculated with Al−Ti−B master alloys can be predicted by [15]

$$\bar{D}=\frac{a}{Q'_{Total}}+\frac{b}{\sqrt[3]{N'}} \tag{12}$$

where a and b are constants.

The constants a and b are determined based on the linear regression analysis by using the experimental average sizes of α(Al) grains in the CP-Al samples inoculated with 0.0154% TiB_2 and different amounts of solute Ti (Group 1 in Table 2). The results indicate that a and b respectively equal 100.7 μm·K and 5.3. Equation (12) is then used to calculate the average size of α(Al) grains in the CP-Al samples inoculated by 0.0154% TiB_2 + 0.0038% Ti (Group 2 in Table 2) with different holding time of the melt, as shown in Fig. 6. The calculated average sizes of α(Al) grains by considering and neglecting the kinetic behaviours of the TiB_2 particles in the melt are quite different, and the former one agrees better with the experimental ones, indicating that the effect of the kinetic behaviour of the TiB_2 particles on the grain refinement cannot be negligible.

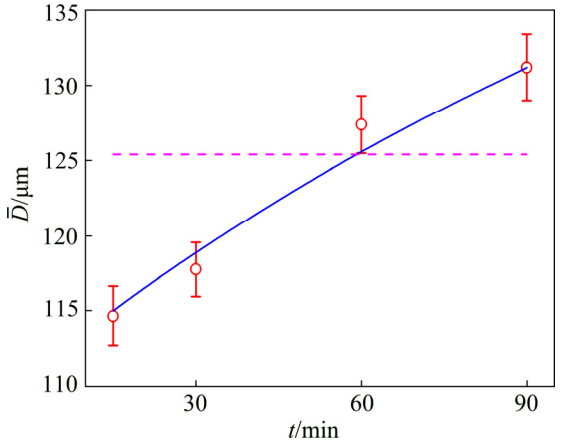

Fig. 6 Experimental (open circles) and calculated average size of α(Al) grains in CP-Al with addition of 0.0154% TiB_2 + 0.0038% Ti by using Q'_{Total} and N' (solid line) and Q_{Total0} and N_0 (dashed line) vs holding time at 983 K

5 Conclusions

(1) When Al−Ti−B master alloy is added to the Al melt, TiB_2 particles may dissolve and coarsen during the holding period and grow during the cooling period of the Al melt.

(2) The average sizes of α(Al) grains by considering and neglecting the kinetic behaviour of TiB_2 particles are calculated. The former one agrees better with the experimental ones.

(3) Solute Ti inhibits the dissolution/growth/coarsening behaviours of the TiB_2 particles and the inhibitory effect increases with the solute Ti content increasing.

References

[1] CHEN Xiang, HUANG Guang-sheng, LIU Shuai-shuai, HAN Ting-zhuang, JIANG Bin, TANG Ai-tao, ZHU Yun-tian, PAN Fu-sheng. Grain refinement and mechanical properties of pure aluminum processed by accumulative extrusion bonding [J]. Transactions of Nonferrous Metals Society of China, 2019, 29: 437−447.

[2] JING Li-jun, PAN Ye, LU Tao, PI Jin-hong, GU Teng-fei. Nucleation potency prediction of LaB_6 with E2EM model and its influence on microstructure and tensile properties of

Al−7Si−0.3Mg alloy [J]. Transactions of Nonferrous Metals Society of China, 2018, 28: 1687−1694.

[3] ZHANG Li-li, JIANG Hong-xiang, ZHAO Jiu-zhou, HE Jie. Microstructure and grain refining efficiency of Al−5Ti−1B master alloys prepared by halide salt route [J]. Journal of Materials Processing Technology, 2017, 246: 205−210.

[4] LI Hong-ying, LI De-wang, ZHU Zhi-xiang, CHEN Bao-an, CHEN Xin, YANG Chang-long, ZHANG Hong-yu, KANG Wei. Grain refinement mechanism of as-cast aluminum by hafnium [J]. Transactions of Nonferrous Metals Society of China, 2016, 26: 3059−3069.

[5] GUO Hong-min, ZHANG Ai-sheng, YANG Xiang-jie, YAN Ming-ming. Grain refinement of Al−5%Cu aluminum alloy under mechanical vibration using meltable vibrating probe [J]. Transactions of Nonferrous Metals Society of China, 2014, 24: 2489−2496.

[6] FAN Z, WANG Y, ZHANG Y, QIN T, ZHOU X R, THOMPSON G E, PENNYCOOKC T, HASHIMOTO T. Grain refining mechanism in the Al/Al−Ti−B system [J]. Acta Materialia, 2015, 84: 292−304.

[7] LI Jie-hua, YANG Guang-yu, HAGE FREDRIK S, CHEN Zong-ning, WANG Tong-min, RAMASSE QUENTIN M, SCHUMACHER P. Heterogeneous nucleation of Al on AlB_2 in Al−7Si alloy [J]. Materials Characterization, 2017, 128: 7−13.

[8] LI Nan, LIU Xiao-jing, WANG Qing-zhou, CUI Chun-xiang, YIN Fu-xing, JI Xiang-wei, JIAO Zhi-xian. Effect of combined addition of Al−Ti−B ribbon and Zr element on the microstructure, mechanical and damping properties of ZA22 alloy [J]. Materials and Design, 2017, 127: 97−105.

[9] RATHI S K, SHARMA A, SABATINO M. Performance of Al−5Ti−1B master alloy after ball milling on minimizing hot tearing in Al−7Si−3Cu Alloy [J]. Transactions of the Indian Institute of Metals, 2017, 70: 827−831.

[10] MAXWELL I, HELLAWELL A. A simple model for grain refinement during solidification [J]. Acta Metallurgica, 1975, 23: 229−237.

[11] GREER A L, BUNN A M, TRONCHE A, EVANS P V, BRISTOW D J. Modeling of inoculation of metallic melts: Application to grain refinement of aluminium by Al−Ti−B [J]. Acta Materialia, 2000, 48: 2823−2835.

[12] QUESTED T E, GREER A L. Grain refinement of Al alloys: Mechanisms determining as-cast grain size in directional solidification [J]. Acta Materialia, 2005, 53: 4643−4653.

[13] QUESTED T E, GREER A L. The effect of the size distribution of inoculant particles on as-cast grain size in aluminium alloys [J]. Acta Materialia, 2004, 52: 3859−3868.

[14] EASTON M A, STJOHN D H. A model of grain refinement incorporating alloy constitution and potency of heterogeneous nucleant particles [J]. Acta Materialia, 2001, 49: 1867−1878.

[15] EASTON M A, STJOHN D H. An analysis of the relationship between grain size, solute content, and the potency and number density of nucleant particles [J]. Metallurgical and Materials Transactions A, 2005, 36: 1911−1919.

[16] EASTON M A, STJOHN D H. Improved prediction of the grain size of aluminium alloys that includes the effect of cooling rate [J]. Materials Science and Engineering A, 2008, 486: 8−13.

[17] QIAN M, CAO P, EASTON M A, MCDONALD S D, STJOHN D H. An analytical model for constitutional supercooling-driven grain formation and grain size prediction [J]. Acta Materialia, 2010, 58: 3262−3270.

[18] EASTON M A, STJOHN D H. Partitioning of titanium during solidification of aluminium alloys [J]. Materials Science and Technology, 2000, 16: 993−1000.

[19] WANG Tong-min, CHEN Zong-ning, FU Hong-wang, GAO Lei, LI Ting-ju. Grain refinement mechanism of pure aluminium by inoculation with Al−B master alloys [J]. Materials Science and Engineering A, 2012, 549: 136−143.

[20] SIGWORTH G K. The grain refining of aluminium and phase relationships in the Al−Ti−B system [J]. Metallurgical Transactions A, 1984, 15: 277−282.

[21] ZHAO Jiu-zhou, RATKE L, JIA Jun, LI Qing-chun. Modeling and simulation of the microstructure evolution during a cooling of immiscible alloy in the miscibility gap [J]. Journal of Materials Processing Technology, 2002, 18: 197−205.

[22] HE Jie, ZHAO Jiu-zhou, RATKE L. Solidification microstructure and dynamics of metastable phase transformation in undercooled liquid Cu−Fe alloys [J]. Acta Materialia, 2006, 54: 1749−1757.

[23] ZHAO Jiu-zhou, LI Hai-li, ZHANG Xian-fei, HE Jie, RATKE L. Microstructure evolution during a liquid-liquid decomposition under the common action of the nucleation, growth and Ostwald ripening of droplets [J]. International Journal of Materials Research, 2009, 100: 1−7.

[24] GALE W F, TOTEMEIR T C. Smithells metals reference book [M]. 8th ed. Oxford: Butterworth−Heinemann, 2004.

[25] ZHANG Li-li, ZHENG Qiu-ju, JIANG Hong-xiang, ZHAO Jiu-zhou. Interfacial energy between Al melt and TiB_2 particles and efficiency of TiB_2 particles to nucleate α-Al [J]. Scripta Materialia, 2019, 160: 25−28.

[26] IIDA T, GUTHRIE R I L. The physical properties of liquid metals [M]. Oxford: Clarendon Press, 1993.

[27] GUO Ming-xing, SHEN Kun, WANG Ming-pu. Relationship between microstructure, properties and reaction conditions for Cu−TiB_2 alloys prepared by in situ reaction [J]. Acta Materialia, 2009, 57: 4568−4579.

[28] LIU Dong-ming, ZHAO Jiu-zhou, YE Heng-qiang, Modeling of the solidification of gas-atomized alloy droplets during spray forming [J]. Materials Science and Engineering A, 2004, 372: 229−234.

[29] FEUERBACHER B, HAMACHER H, NAUMANN R. Materials sciences in space: A contribution to the scientific basis of space processing [M]. Berlin: Springer-Verlag, 1986.

[30] BALLUFFI R W, ALLEN S M, CARTER W C. Kinetics of materials [M]. Massachusetts: Wiley-Interscience, 2005.

TiB_2 粒子在 Al 熔体中的动力学行为及其对铝合金晶粒细化效果的影响

张丽丽[1]，江鸿翔[1]，何 杰[1,2]，赵九洲[1,2]

1. 中国科学院 金属研究所 师昌绪先进材料创新中心，沈阳 110016；
2. 中国科学技术大学材料科学与工程学院，沈阳 110116

摘 要：实验研究铝合金熔体中 TiB_2 粒子动力学行为及其对铝合金晶粒细化效果的影响，建立描述自 TiB_2 粒子加入合金熔体至合金熔体凝固过程中 TiB_2 粒子的动力学模型。结果表明，TiB_2 粒子在 Al 熔体中不稳定，在保温阶段发生溶解和熟化行为，并在熔体冷却阶段长大；TiB_2 粒子的动力学行为影响其数量密度和铝合金晶粒细化效果；溶质 Ti 对 TiB_2 粒子的溶解、熟化及快速长大行为具有抑制作用。

关键词：TiB_2 粒子；动力学行为；晶粒细化；铝合金

(Edited by Bing YANG)